# Structural Origin of Circularly Polarized Iridescence in Jeweled Beetles

Vivek Sharma,[1,2] Matija Crne,[2,3] Jung Ok Park,[1,2] Mohan Srinivasarao[1,2,3]

The iridescent metallic green beetle, *Chrysina gloriosa*, which selectively reflects left circularly polarized light, possesses an exoskeleton decorated by hexagonal cells (~10 μm) that coexist with pentagons and heptagons. The fraction of hexagons decreases with an increase in curvature. In bright field microscopy, each cell contains a bright yellow core, placed in a greenish cell with yellowish border, but the core disappears in dark field. With use of confocal microscopy, we observe that these cells consist of nearly concentric nested arcs that lie on the surface of a shallow cone. We infer that the patterns are structurally and optically analogous to the focal conic domains formed spontaneously on the free surface of a cholesteric liquid crystal. These textures provide the basis for the morphogenesis as well as key insights for emulating the intricate optical response of the exoskeleton of scarab beetles.

Iridescent beetles, butterflies, certain sea organisms, and many birds derive their color from the interaction of light with the structure or morphology that is imprinted on their exoskeletons (*1*–*5*). The bright and varied colors of beetles have been of interest to scientists (*2*, *6*–*8*), but they also have a long and interesting history as "jewel beetles," which were used in textiles or ornaments (*9*) in many Asian countries. The study of photonics in nature reveals beautiful and diverse examples of subwavelength structural features that create observed colors through thin layered or multilayered interference, diffraction, zero order diffraction, and light scattering (*1*–*5*) and often with contributions from pigmentation as well. The complexity of the patterns is in part determined genetically, but the final development and control is related to the conditions during the formation of the pattern (*10*, *11*). The physical and chemical aspects of morphogenesis can be unraveled by studying the patterns in nature and analyzing their analogs in equilibrium and nonequilibrium patterns formed in condensed matter (*12*–*15*). The quest for miniature optical devices and photonics is most likely to benefit from the study of bioengineered organs and organelles of the biological world. Rational design requires one to understand how basic structural units interact with light and how they can be fabricated by either self-assembly or a top-down approach.

In this context, we have been examining the structure on the exocuticle of the beetle *Chrysina gloriosa* (or *Plusiotis gloriosa*), which selectively reflects left circularly polarized light and possesses a brilliant metallic appearance (Fig. 1). If left circularly polarized light is blocked by the use of a quarter wave plate and a polarizer, as shown in Fig. 1B, the beetle loses its characteristic bright green reflection. The ability of certain species of beetles to reflect circularly polarized light has been investigated for nearly a century (*16*–*20*), since it was first reported by Michelson (*6*). Recently Goldstein (*7*) summarized the history of optical measurements made in scarab beetles and performed ellipsometric studies confirming their polarizing behavior. The reflectance of the *C. gloriosa* beetle has a broad halo from 500 to 600 nm with two peaks at 530 (green) and 580 nm (yellow), respectively.

When the exoskeleton of the beetle is observed under an optical microscope, the body appears as a richly decorated mosaic of cusps and color, consisting of a regularly spaced lattice of features that distinguish one species of beetle from the other. In bright field microscopy (Fig. 2), the structure of *C. gloriosa* seems to consist of hexagonal cells (~10 μm), where each cell appears to be green with a bright yellow core or nucleus. We characterized the extent of hexagonal order in patterns by using Voronoi analysis, which is a versatile method for pattern recognition and for modeling the properties of spatial structures (*21*). Although the population of six-sided polygons is the highest, there exist large numbers of five- and seven-sided polygons. If we define $P_n$ to represent the fraction of $n$-sided polygons, we find that $P_5$ decreased from 0.34 at the highly curved head to about 0.19 at the flattest region on the beetles' back, whereas $P_7$ is typically close to 0.13 everywhere else. Although most of the pentagons and heptagons occur in clusters, there are finite numbers of pentagons that occur individually. The number and spatial distribution of polygons characterizes the spatial order. Entropy, $S = -\Sigma P_n \ln P_n$, of the structure was determined for each image. Whereas for perfectly ordered hexagons $P_6 = 1$ and $S = 0$, the value of the entropy on beetle exoskeleton varies between 0.85 and 0.95. Both $P_5$ and entropy are higher in the regions of greater curvature, revealing packing issues on curved surfaces.

The head, thorax, and abdomen of a beetle are all curved, although the radius of curvature, $R$, is large compared with the size of individual cells, $a$, or $R/a >> 1$. Although hexagonal packing provides the most efficient utilization of space on a plane, defects in coordination number are essential for wrapping such tessellations on a sphere (*22*). For example, soccer balls and C60 (fullerenes) contain 12 pentagons in addition to the hexagons that template the curved structure. Because the beetle has a curved body, a certain number of pentagons is expected, but the analysis reveals much higher disorder. According to Nelson (*22*), the energetic cost associated with creating these 12 defects scales as $YR^2$, where $Y$ is the two-dimensional (2D) Young's modulus. Because the cost becomes substantial for systems with large $R/a$, the system creates minimum-energy configurations for the curved substrates by incorporating grain boundaries and defects (*22*–*24*). This results in the faceted morphology of viruses (*22*) and grain boundary scars in colloidosomes (particles packed on a spherical droplet) (*23*). We can infer that the exoskeleton of the beetle possesses imperfect hexagonal, cellular pattern because sixfold triangulations or hexagons are not energetically favored everywhere.

We examined the beetle exoskeleton with use of a laser scanning confocal microscope [Leica TCS SP DMR XE (Leica Microsystems GmbH, Wetzlar, Germany)] and reconstructed a 3D map of the underlying structure by using the auto-

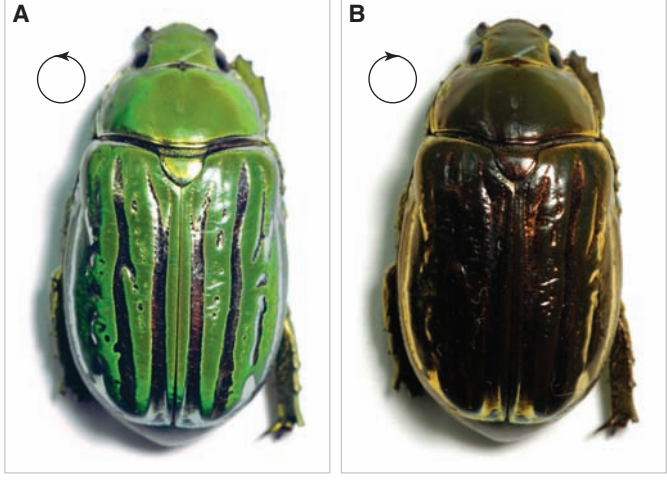


**Fig. 1.** Photographs of the beetle *C. gloriosa*. (**A**) The bright green color, with silver stripes as seen in unpolarized light or with a left circular polarizer. (**B**) The green color is mostly lost when seen with a right circular polarizer.

[1]School of Polymer, Textile, and Fiber Engineering, Georgia Institute of Technology, Atlanta, GA 30332, USA. [2]Center for Advanced Research on Optical Microscopy (CAROM), Georgia Institute of Technology, Atlanta, GA 30332, USA. [3]School of Chemistry and Biochemisty, Georgia Institute of Technology, Atlanta, GA 30332, USA.

fluorescence of the beetle under the excitation of a 488-nm laser. The relief of the cells, when observed under high magnification, consists of bright and dark nearly concentric regions, as shown in Fig. 3, A to C. The fluorescence response from the unidentified fluorophore present in the elytra is dependent on the polarization state and intensity of light that excites it. Hence, the darker regions could point to either changing fluorophore orientation or to a change in the fluorophore concentration. The 3D reconstruction of the images suggests the former: It shows the existence of a microstructure of nested arcs, and the cells seem to have a conical protrusion at the center.

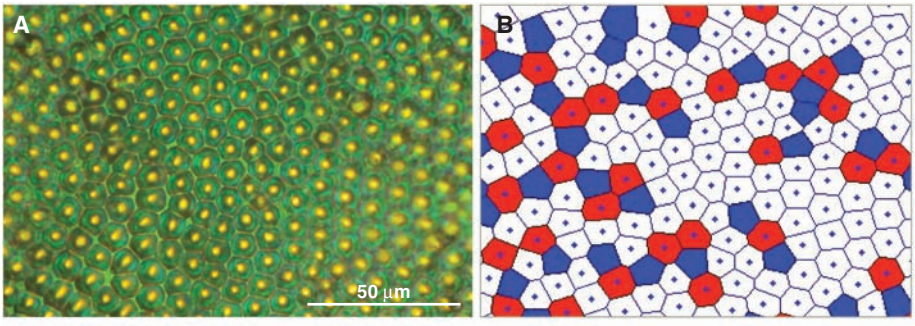


**Fig. 2.** (**A**) An optical micrograph of the exoskeleton of beetle *C. gloriosa* showing bright yellow reflections from the core of each cell (~10 μm in size) and greenish reflection from the edges. (**B**) Voronoi analysis of a section from the corresponding image. Pentagons are colored blue, heptagons are red, and hexagons are white.

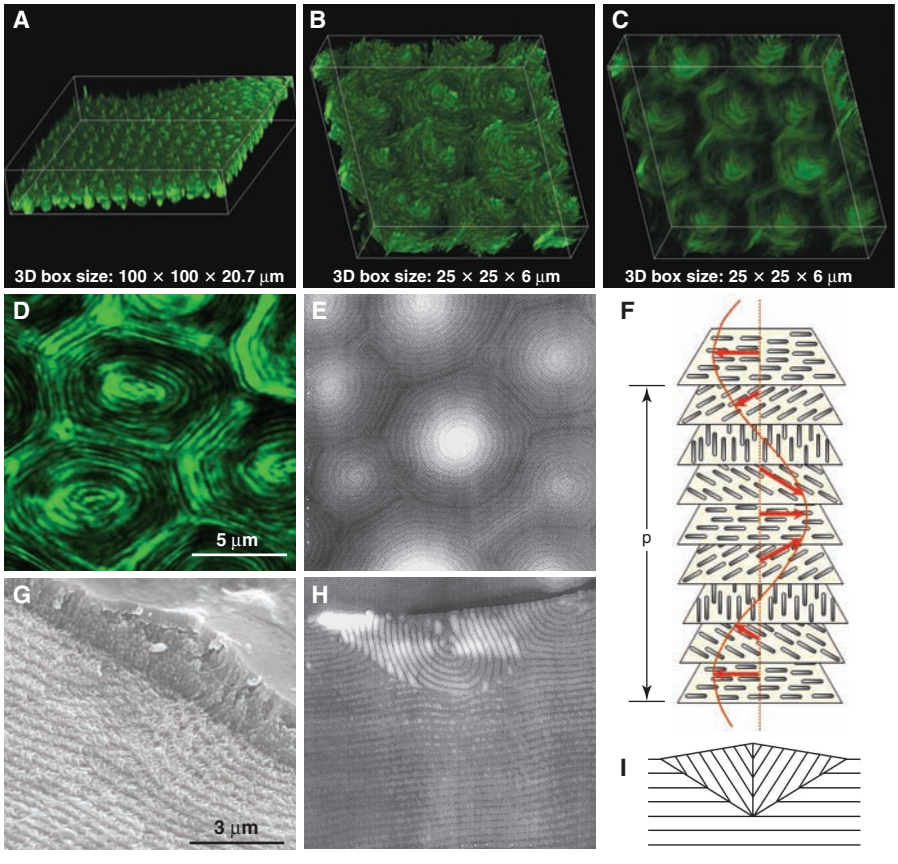


**Fig. 3.** Morphology and microstructure of cellular pattern of *C. gloriosa*. (**A**) An angled view of 3D image at a low magnification reveals upward cones at the center of each cell. (**B** and **C**) Three-dimensional images at higher magnification for limited thickness range in different viewing modes, which may imply that the concentric bright/dark regions are spiraled. (**D**) A typical *x-y* section, showing a relief feature with concentric rings that is resolved only at a high magnification and present only near the free surface. (**E**) An AFM image of the cholesteric focal conic domains at the free surface, showing double spirals that form a shallow cone [from (*25*)]. (**F**) Schematic representation of relative arrangement of chiral mesogens in a cholesteric liquid crystal, stacked in a single twist structure (layers are for illustration purposes only, no lamellar ordering in the *z* direction). (**G**) SEM image shows the nested arcs and a waxy layer on top. (**H**) AFM image of the microtome cut perpendicular to free surface [from (*25*)]. (**I**) Model of focal conic domain adopted from (*25*), showing a cut along the center of the cone, neglecting the exact structure at the center.

The microstructure of the beetle surface (Fig. 3D) resembles the atomic force microscopy (AFM) image of the focal conic domains (Fig. 3E) that spontaneously arise on the free surface of a siloxane oligomer–based cholesteric liquid crystal (*25*). The spiral structure (Fig. 3, A to C) observed in each cell on the beetle exoskeleton also correlates nicely with the conical form observed by Meister *et al*. (*25*) with use of AFM, where the periodic structure resulting from the cholesteric pitch is superimposed on a fat cone (height/maximum diameter ~ 0.01). Likewise the focal conic cholesteric domains are organized in a near-hexagonal packing. Furthermore, our scanning electron microscopy (SEM) image (Fig. 3G) of the beetle exoskeleton bears similarity to the corresponding AFM image (Fig. 3H) obtained for a section microtomed perpendicular to the free surface (*25*), where the underlying layers can be seen clearly.

The selective reflection of circularly polarized light of one-handedness by exocuticle of many beetles has been noted to be similar to the optical response of cholesteric liquid crystals (*16*–*20*). The cholesteric liquid crystal possesses a long-range orientational order described by a unit vector **n**, known as the director, and the equilibrium director structure is a helicoid (*20*, *26*–*28*). The director advances uniformly, tracing a helix of pitch *p* as sketched in Fig. 3F. The presence of helicoidal structure in beetles and other organisms (*2*, *5*, *16*–*20*) is well recognized. Pace (*29*) noticed the helicoid in transmission electron microscopy (TEM) micrographs from of the exoskeleton of *C. gloriosa* and called it a Bouligand structure. Bouligand (*19*, *20*) had carried out an extensive study on the similarity of textures observed in crabs and other organisms to cholesteric liquid crystals and explored their role in morphogenesis. The surfaces produced by the freeze fracture process can possess a relief resulting from the anisotropic propagation of fracture, and the action of a microtome knife produces a topography (studied by using TEM) that depends on the texture of the cut material (*19*, *25*, *30*). But in this study, because we imaged the 3D microstructure of the beetle elytra in a nondestructive fashion with confocal microscopy, the similarity to the cholesteric focal conic texture at the free surface is unmistakable. Interestingly, the confocal image (3D) has a remarkable similarity to the TEM images of *C. gloriosa* by Pace (*29*). Although the helicoidal structure and resulting optical response has been investigated before (*2*, *5*, *18*, *29*), the observed disorder in hexagonal pattern (Fig. 2); details related to microstructure, including resemblance to focal conic domains at the free surface of a cholesterics (Fig. 3); and the

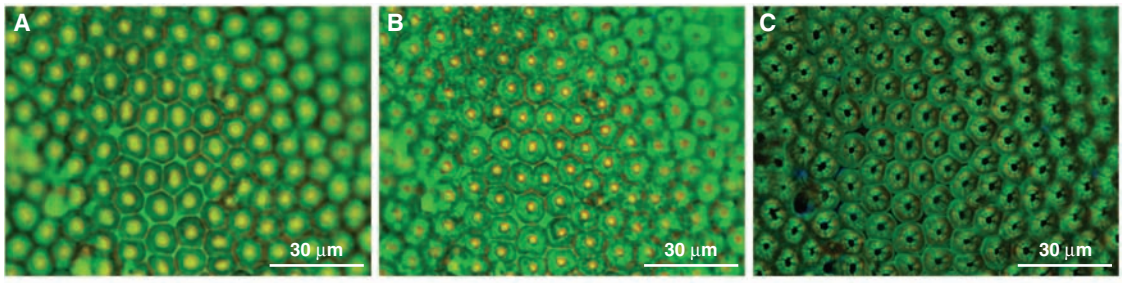


**Fig. 4.** Optical micrographs of the exoskeleton of *C. gloriosa.* Because the surfaces are curved, only the central parts of the images are in focus. (**A**) In bright field, with microscope aperture wide open, to allow a bigger cone of white light. (**B**) In bright field, near-normal incidence obtained by decreasing the aperture. (**C**) In dark field, where near-normal incidence is not present.

intricate optical response of cells (Fig. 4) presented here have not been reported.

Lastly, let us return to the question of the iridescence or angle-dependent color of the beetles (Fig. 4). Because we have limited knowledge of all of the optical and structural parameters necessary for determining the optical response by ray tracing, we can put forward only phenomenological arguments. Because of its chiral and periodic helicoidal structure, the cholesteric phase with a pitch comparable to the wavelength of visible light shows Bragg-like reflection for normal incidence, peaked at wavelength, $\lambda_0$, given by $\lambda_0 = np$, where $n$ is the average refractive index (*26*, *28*, *31*). The spectral width of the reflection peak for a pure cholesteric phase is related to birefringence ($\Delta n = n_e - n_o$) by $\Delta\lambda = p\Delta n$ (*26*, *28*, *31*), where $n_o$ and $n_e$ are the refractive indices for polarizations perpendicular (ordinary) and parallel (extraordinary) to the axis of anisotropy, respectively. For oblique incidence at an angle $\phi$, the reflection for a helical axis oriented at some angle $\theta$ with respect to surface normal, the condition for first-order Bragg reflection is modified to $\lambda = np\cos(\phi - \theta)$, and additional effects appear (*31*). When we look at the beetle structure in the white light in a reflection microscope, the Bragg-like reflection is yellow at the center of the cell and green elsewhere. When the range of incidence angles is increased by increasing the aperture size (Fig. 4A), the locus of the yellow reflection expands (in comparison to Fig. 4B), implying that, by increasing the angle of incidence of beams over the beetle, $(\phi - \theta)$ becomes smaller; hence, $\cos(\phi - \theta)$ increases, and thus a longer wavelength (yellow as opposed to green) satisfies the condition. In the dark field, when only large angles of incidence are possible, $\phi - \theta$ is large; hence, the $\cos(\phi - \theta)$ term near the center gets even smaller, leading to extinction of color at the center (Fig. 4C). This red shift in wavelength on increasing angle of incidence is also discernible in spectral analysis from the green region, where the peak wavelength increases from 525 nm at normal incidence to 556 nm in dark field illumination. In this analysis, we have neglected the change in incident angle at the helix resulting from refraction at wax-air interface. However, this does not perturb the arguments for the optics presented here.

In the optical studies by Jewell *et al*. (*32*) on *P. boucardi* beetles, similar hexagonal cells are observed to show dark centers in dark field and to turn yellow in bright field. For *P. resplendens* (*17*), *P. boucardi* (*32*), and the New Zealand manuka beetle (*33*), the presence of chiral reflectors with two different pitches satisfying Bragg reflection was cited as responsible for color. Similarly, Brink *et al*. (*34*) simulated the reflected spectrum of the red and green scarabaeid beetle *Gymnopleurus virens* by using a perturbed cholesteric structure that has an abrupt jump in pitch and in rotation of the cholesteric structure. We propose that the focal conic domains formed at the free surface of a cholesteric liquid crystal can create the perturbed cholesteric relief that can account for the color and the morphology of the exocuticle of the scarabaeid beetles. The selective reflection of the cholesteric phases can be modified by a change in pitch, birefringence, cell thickness, angle of incidence, and polarization as well as by the orientation of helical axis (*26*–*28*, *31*, *35*), and the scarabeid beetles, examples of photonic structures in biology, have used a multiplicity of these possibilities (*17*, *19*, *32*–*34*). Although the details of morphogenesis will influence the exact nature of the microstructure and observed color for a particular beetle, we infer that each of these mechanisms provides us with inspiration to the design of chiro-optical devices. In fact, inorganic analogs that mimic optical effects of scarabeid beetles are already being developed (*8*). The desired optical response can be achieved from self-assembly akin to biological systems either by incorporating a bistable cholesteric phase formed because of free surface, by using controlled anchoring, or by using structures with variable pitch [say by having a concentration gradient of nematic blended into a cholesteric fluid (*36*)].

### References and Notes

1. H. Ghiradella, *Appl. Opt.* **30**, 3492 (1991).
2. M. Srinivasarao, *Chem. Rev.* **99**, 1935 (1999).
3. P. Vukusic, J. R. Sambles, *Nature* **424**, 852 (2003).
4. A. R. Parker, *J. Opt. A Pure Appl. Opt.* **2**, R15 (2000).
5. S. Bertheier, *Iridescences: The Physical Color of Insects* (Springer, New York, 2007).
6. A. A. Michelson, *Studies in Optics* (Univ. of Chicago Press, Chicago, IL, 1927).
7. D. H. Goldstein, *Appl. Opt.* **45**, 7944 (2006).
8. S. Lowrey, L. De Silva, I. Hodgkinson, J. Leader, *J. Opt. Soc. Am. A Opt. Image Sci. Vis.* **24**, 2418 (2007).
9. V. Z. Rivers, in *Les Insectes Dans la Tradition Orale/Insects in Oral Literature and Traditions*, E. Motte-Florac, J. M. C. Thomas, Eds., SELAF 407, Ethnosciences 11 (Peeters, Walpole, MA, 2003), pp. 163–174.
10. D. A. Thompson, *On Growth and Form* (Cambridge Univ. Press, Cambridge, 1961).
11. P. S. Stevens, *Patterns in Nature* (Little, Boston, MA, 1974).
12. A. M. Turing, *Philos. Trans. R. Soc. London Ser. B* **237**, 37 (1953).
13. P. Ball, *The Self-Made Tapestry: Pattern Formation in Nature* (Oxford Univ. Press, Oxford, 1999).
14. M. C. Cross, P. C. Hohenberg, *Rev. Mod. Phys.* **65**, 851 (1993).
15. A. J. Koch, H. Meinhardt, *Rev. Mod. Phys.* **66**, 1481 (1994).
16. A. C. Neville, S. Caveney, *Biol. Rev. Cambridge Philos. Soc.* **44**, 531 (1969).
17. S. Caveney, *Proc. R. Soc. London Ser. B* **178**, 205 (1971).
18. A. C. Neville, *Biology of Fibrous Composites: Development Beyond the Cell Membrane* (Cambridge Univ. Press, Cambridge, 1993).
19. Y. Bouligand, *C. R. Chim.* **11**, 281 (2008).
20. Y. Bouligand, in *Bifurcation Theory, Mechanics, and Physics*, C. P. Bruter, A. Arangol, A. Lichenrowicz, Eds. (Riedel, Dordecht, Netherlands, 1983).
21. A. Okabe, B. Boots, K. Sugihara, S. N. Chiu, *Spatial Tessellations: Concepts and Applications of Voronoi Diagrams* (Wiley, New York, 2000).
22. D. R. Nelson, *Proc. Int. Sch. Phys. Enrico Fermi* **155**, 365 (2004).
23. A. R. Bausch *et al*., *Science* **299**, 1716 (2003).
24. V. Vitelli, J. B. Lucks, D. R. Nelson, *Proc. Natl. Acad. Sci. U.S.A.* **103**, 12323 (2006).
25. R. Meister, M. A. Halle, H. Dumoulin, P. Pieranski, *Phys. Rev. E Fluids Relat. Interdiscip. Topics* **54**, 3771 (1996).
26. P. G. de Gennes, J. Prost, *Int. Ser. Monogr. Phys* **83**, 263 (1995).
27. M. Kleman, O. D. Lavrentovich, *Soft Matter Physics: An Introduction* (Springer-Verlag, New York, 2003).
28. P. Oswald, P. Pieranski, in *Nematic and Cholesteric Liquid Crystals*, G. W. Gray, J. W. Goodby, A. Fukuda, Eds. (Taylor and Francis, Boca Raton, FL, 2005), pp. 415–492.
29. A. Pace Jr., *Science* **176**, 678 (1972).
30. D. W. Berreman, S. Meiboom, J. A. Zasadzinski, M. J. Sammon, *Phys. Rev. Lett.* **57**, 1737 (1986).
31. V. A. Belyakov, V. E. Dmitrienko, *Optics of Chiral Liquid Crystals* (Harwood, New York, 1989).
32. S. A. Jewell, P. Vukusic, N. W. Roberts, *N. J. Phys.* **9**, 99 (2007).
33. L. De Silva *et al*., *Electromagnetics* **25**, 391 (2005).
34. D. J. Brink, N. G. van der Berg, L. C. Prinsloo, I. J. Hodgkinson, *J. Phys. D* **40**, 2189 (2007).
35. W. D. St. John, W. J. Fritz, Z. J. Lu, D. K. Yang, *Phys. Rev. E* **51**, 1191 (1995).
36. D. J. Broer, J. Lub, G. N. Mol, *Nature* **378**, 467 (1995).
37. M.S. acknowledges support from NSF (DMR-0706235) and useful discussions with L. Tolbert, A. Rey, P. Collings, and H. Ghiradella.

### Supporting Online Material

www.sciencemag.org/cgi/content/full/325/5939/449/DC1
Materials and Methods
SOM Text
References

9 February 2009; accepted 5 June 2009
10.1126/science.1172051